Precision Measurement of the g Factor of the Free Positron*

John R. Gilleland† and Arthur Rich
The Harrison M. Randall Laboratory of Physics, The University of Michigan, Ann Arbor, Michigan 48104
(Received 23 August 1971)

In this paper we describe a precision measurement of the g factor of the free positron. The basic experimental technique is that developed by Rich and Crane in an earlier positron experiment: A group of positrons from a Co^{58} source is confined in a magnetic mirror trap. On emission from the source, the positron beam is polarized parallel to its average velocity $\langle\vec{v}\rangle$, with polarization $\vec{P}=\langle\vec{v}\rangle/c$. While in the field the beam undergoes cyclotron orbital motion at an angular frequency ω_c. Simultaneously $\vec{P}$ precesses at an angular frequency ω_s, i.e., $\vec{P}$ rotates about $\vec{v}$ at the difference frequency $\omega_D=\omega_s-\omega_c$. After a controlled length of time, the particles are ejected from the trap and sent into a polarimeter, this being a device whose response is proportional to the helicity, $\vec{v}\cdot\vec{P}/|\vec{v}||\vec{P}|$. The recorded polarimeter output vs trapping time is fitted to a cosine curve and the best-fit frequency is taken as ω_D. This measurement of ω_D, when combined with a measurement of the time-averaged field B experienced by the positrons in the trap, is the basis of the experiment. More explicitly, if the g factor is written as $g=2(1+a)$, where a is the g factor anomaly, then $a=(m_0c/eB)\omega_D$. The principal difference between the present experiment and previous work is the use of a pulsed coil instead of a dc magnet to generate a 10-kG magnetic field used in the polarimeter. Fringe fields from the dc magnet caused severe drifting of the trapped beam, a problem which has been overcome by use of the coil. The longer trapping times now obtained account for a factor of 5 improvement in measurement accuracy. The result of our experiment may be written as $a=(11\,603\pm12)\times10^{-7}$. Invariance under TCP requires equality of the electron and positron g factors. Our results, when compared with previous electron measurements, serve to confirm this prediction at the 1-ppm level in the g factor. Furthermore, since the μ^+ and μ^- g factors are equal to within 0.7 ppm, any violation of TCP which manifests itself in a lepton-antilepton g factor asymmetry is ruled out at the 1-ppm level.

I. INTRODUCTION

The purpose of this article is to describe a precision measurement of the g factor of the free positron. This experiment is the latest in a long series of positron and electron g-factor measurements performed in this laboratory over the last two decades.[1] A preliminary account of the work may be found in Ref. 2.

Emphasis upon the verification of quantum electrodynamic theory characterized the electron g-factor determinations. The present measurement, however, is best described in terms of a comparison experiment, in which our result is to be compared with the more accurately known electron g factor. The motivation for such a comparison is clear. It is a consequence of the TCP theorem that the g factor, mass, lifetime, etc., of particle and antiparticle are equal. Since measurements have shown that the μ^+ and μ^- g factors are equal to within 0.7 ppm,[3] it was hoped that our experiment would complete such g-factor comparisons at the 1-ppm level for leptons.

The only direct measurement of the g factor of the free positron previously reported is due to Rich and Crane.[4] If the g factor is written in terms of the anomaly a as $g=2(1+a)$, then the result of their experiment is written as $a(e^+)_E=(11\,680\pm55)\times10^{-7}$. The best experimental value of the electron anomaly reported to date results from work by Wesley and Rich,[5] who report $a(e^-)_E=(1\,159\,658\pm3.5)\times10^{-9}$. The previous result for $a(e^-)_E$, by Wilkinson and Crane,[6] as revised by Henry and Silver and Rich,[6] was $a(e^-)_E=(1\,159\,549\pm30)\times10^{-9}$. Our errors are approximately 100 times these. Consequently we may compare our result of $a(e^+)_E=(11\,603\pm12)\times10^{-7}$ with either experimental number for $a(e^-)_E$, or with the theoretical value, which is given by

$$a(e^+)_T=a(e^-)_T=0.5(\alpha/\pi)-0.32848\,(\alpha/\pi)^2$$
$$=(1\,159\,644\pm2)\times10^{-9}\,. \qquad (1)$$

The error in a_T is assumed to be due only to error in α, which we take as $\alpha^{-1}=137.036\,08\pm0.000\,26$.[7] The $(\alpha/\pi)^3$ term in the expansion has been omitted because its effect is negligible at the level of accuracy which we report.

II. METHOD OF MEASUREMENT

A. Difference of Frequency

Consider a charged particle with spin $\vec{S}$, charge e, rest mass m_0, and magnetic moment $\vec{\mu}$

$= ge\vec{S}/2m_0c$, moving perpendicular to a uniform magnetic field $\vec{B}$. The particle rotates at the cyclotron angular frequency $\omega_c = eB/\gamma m_0 c$, $\gamma = (1 - v^2/c^2)^{-1/2}$, while its spin precesses at the frequency $\omega_s = \omega_c(1 + a\gamma)$. The term $a\gamma$ is due to the Thomas precession caused by the cyclotron motion. In this simple case we may describe the spin motion graphically. At a given point on the cyclotron orbit, the projection of $\vec{S}$ onto a fixed direction varies as $\cos\omega_D t$, where ω_D is the beat or difference frequency. It is given by

$$\omega_D = \omega_s - \omega_c = a\, eB/m_0 c = a\omega_0 \ . \qquad (2)$$

The fact that ω_D is, under these conditions, rigorously independent of energy makes possible the entire series of high-precision lepton g-2 experiments described in Sec. I. The ideal conditions under which Eq. (2) holds true are not exactly fulfilled in our experiment. The required small corrections will be discussed in Sec. IID.

B. General Technique

The method for measurement of ω_0 and ω_D may be seen from Fig. 1: A "bunch" of positrons from a group of four Co^{58} sources is confined in a magnetic mirror trap. On emission from the sources, the "beam" is already polarized parallel to its "average" velocity $\langle\vec{v}\rangle$, with polarization $\vec{P} = \langle\vec{v}\rangle/c$. While the particles are in the trap, we may describe the motion of $\vec{P}$ to a high approximation as a precession about $\vec{v}$ at ω_D. After a measured length of time the positrons are ejected from the trap into a "polarimeter." By a polarimeter we mean a device which has a linear response to the projection of $\vec{P}$ onto a fixed direction $\hat{h}$ in the laboratory. Since the beam always enters the polarimeter in the same direction, independently of trapping time, this projection differs by only a constant angle from $\vec{P}\cdot\vec{v}/|v|\,|P|$. Therefore the projection is proportional to $\cos(\omega_D T + \varphi)$, where T is the time the positrons are trapped and φ is a phase constant.

To obtain ω_D we measure the output of the polarimeter as a function of T. The data, when fitted to a sinusoid, allow us to infer the value of ω_D. A map of the field B in the trapping region then allows calculation of ω_0. The constant e/m_0c for the positron has been measured to sufficient accuracy.[8]

C. Polarimeter

The polarimeter used here is based upon the formation and decay of positronium Ps in a 10-kG magnetic field $\vec{B}_p$.[9] On ejection from the trap, the positrons are made to stop in a plastic scintillator situated in the field. This field defines the the fixed direction $\hat{h}$ discussed above. Roughly half of the entering positrons form Ps. The fast coincidence circuit counts the number of Ps atoms which decay during a given time interval $t = t_2 - t_1$. This number depends on the angle θ between $\vec{P}$ and $\hat{h}$, and on t_1 and t_2. It shall be denoted as $N(\theta, t_1, t_2)$. All other parameters which can affect N are either averaged over or held constant during the experiment. The theoretical expression for $N(\theta, t_1, t_2)$ when $t_2 \gg t_1$ is

$$N(\theta, t_1, t_2) = N(\theta, t_1)$$

$$= \tfrac{1}{4}N_0\left[2\,e^{-\Lambda_{1,0}t_1} + e^{-\Lambda'_{1,0}t_1} + e^{-\Lambda'_{0,0}t_1}\right.$$

$$\left. - xP(1+x^2)^{-1/2}\cos\theta\,(e^{-\Lambda'_{1,0}t_1} - e^{-\Lambda'_{0,0}t_1})\right] \ . \qquad (3)$$

Here $\Lambda_{1,0}$ is the unperturbed $m = 0$ triplet decay rate, $\Lambda'_{1,0}$ is the field-perturbed $m = 0$ triplet decay rate, and $\Lambda'_{0,0}$ is the field-perturbed singlet decay rate. The quantity N_0 is the total number of incident positrons and $x = 4\mu_B B_p/(E_{1,0} - E_{0,0})$. For the

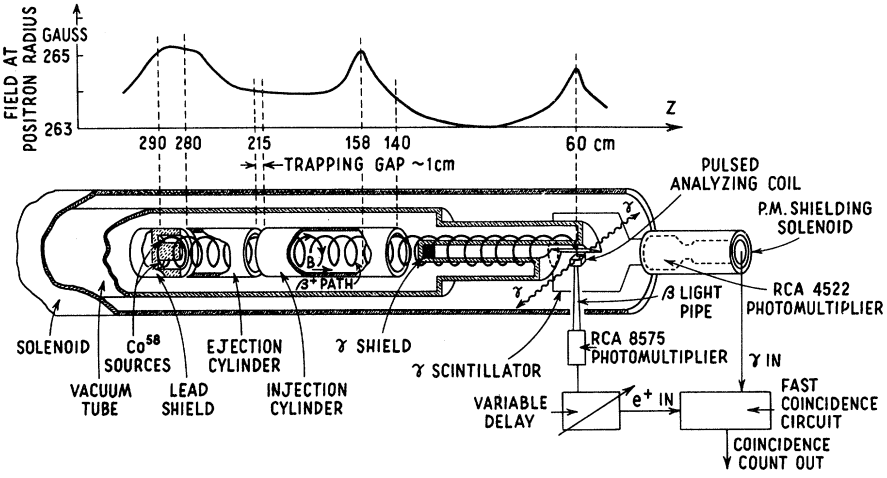

FIG. 1. Schematic diagram of the positron g-factor experiment.

parameters of our experiment, expression (3) for the output of a perfect coincidence counter becomes

$$N(\theta) = 0.3 N_0 (1 - 0.06 \cos\theta) \quad (4)$$

or equivalently

$$N(T) = 0.03 N_0 [1 - 0.06 \cos(\omega_D T + \varphi)]. \quad (5)$$

For a more complete discussion of Ps decay the reader is referred to the Appendix, while the effect of the finite time resolution of our coincidence counter is discussed in Sec. III. The coincidence time resolution considerably lowers the 6% asymmetry expected from Eq. (4).

D. Correction Terms

Equation (2) must be corrected to account for the necessarily inhomogeneous magnetic trapping field, the finite axial velocity of the particles in the well, and the effect of possible stray radial electric fields (E_r). The result[10] is that, to the required accuracy,

$$a = \frac{[\omega_D]}{[\omega_0]} + \frac{\frac{1}{2}a[v_z^2]}{c^2} + \frac{1}{\beta\gamma^2}\frac{[E_r]}{[B_z]}. \quad (6)$$

Here the symbol [ ] denotes time average, i.e., we need the value of the quantities ω_D, ω_0, v_z^2, and E_r averaged over one period in the well. This assumes no secular effects in the orbital motion, an assumption which has been justified experimentally (Sec. III).

III. APPARATUS

A. Trapping Field

The solenoid used to generate the 262-G trapping field is approximately 3.4 m long and 0.6 m in diameter. It is constructed of an even number of layers of No. 10 cotton and enamel insulated copper wire wound on a rigid aluminum spool. The field regulating system is made up of a series current regulator and a parallel NMR regulator. The sensing element of the fine regulator uses a proton resonance head containing a 0.1M cupric chloride solution. The system is essentially the same as that used in previous measurements, and details of its operation have already been published elsewhere.[11] Fluctuations in the field were held to less than 75 ppm during the nine months of final experimentation and data collection.

B. Source and Beam Collimation

The initial activity of each of the four Co^{58} sources was about 250 mCi. Although Co^{58} has a half-life of only 71 days, it was nevertheless found to be the most suitable positron source available when cost and fabrication requirements were considered.

Each source was made by electroplating carrier-free Co^{58} onto a 2×7-mm copper foil. The combination was then heated in a hydrogen furnace. This caused the Co^{58} to permeate the copper foil and yielded a mechanically stable source capable of retaining its integrity under vacuum. Since the foil is only 6 mg/cm^2 in thickness, there is no significant depolarization of the beam on emission from the source.[12] Also, since the source foils were mounted on low-Z (beryllium) backings, backscattering has been effectively eliminated as a source of depolarization.[12]

The sources are situated in a lead collimator as shown in Fig. 1. Only particles on helical trajectories with radii ranging from 7.56 to 7.64 cm are unobstructed by the collimator and can enter the trapping region. For a 262-G trapping field, this range of radii sets the particle energy at 273 ± 21 keV, corresponding to a polarization $|P| = 0.76 \pm 0.02$.

C. Trapping

The trap is produced by the magnetic mirrors at $z = 160$ cm and $z = 260$ cm in Fig. 1. These mirrors act as potential hills as far as the axial motion of the positrons is concerned. Specifically if $T_z(z) \equiv \frac{1}{2}\gamma m_0 v_z^2$, then under conditions to be discussed later (Sec. IV) we have

$$T_z(z) - T_z(z_0) = \text{const} \times [B_z(z_0) - B_z(z)]. \quad (7)$$

Here z_0 is an arbitrary reference point chosen for convenience. The constant is 866 eV/G in our application, so that the height of the inject and eject hills are 1500 and 1400 eV, respectively.

Trapping is accomplished by pulsing the injection cylinder 600 V positive. A positron which crosses the gap while the pulse is applied will experience a retarding axial electric field. Some particles will lose enough axial momentum to cause reflection at the right-hand mirror. If the pulse is removed before the particle recrosses the gap in the opposite direction, the particle never regains its lost axial momentum and is thus trapped. Ejection occurs when the ejection cylinder is pulsed positive. If a particle is in the left half of the well when the pulse is applied, it will gain axial momentum when it crosses the gap. The particle then travels down the solenoid on a helical trajectory to the polarimeter.

The brass inject and eject cylinders are 25 cm in diam and of sufficient length to overlap the ends of the well by about 13 cm. The cylinders are connected to ground through 200-Ω resistors. The 0.5-μsec-wide 600-V-high inject and eject pulses are generated by two type 350 Velonex hard-tube pulsers.

D. Polarimeter Field

The use of a pulsed polarimeter field is the major

difference between this and the previous positron measurement. Formerly positrons were extracted from the solenoid and brought to a dc polarimeter magnet. Fringe fields from the magnet caused severe drifting of the trapped beam and limited the trapping time to only eight useful cycles of the ω_D curve. In the new arrangement, a trapping time of over 110 μsec, corresponding to 80 cycles of the ω_D curve, is feasible. This accounts for our improved accuracy.

Elimination of the ejection system also increases the over-all efficiency of the apparatus. The ratio of the number of positrons counted to the number originally emitted by the source is up by a factor of about 4. Alternate methods of reducing the fringe fields in the trap, such as an increase in the distance between the magnet and well, can give no such increase in efficiency.

Pulsing of the polarimeter field begins about 1.5 μsec before ejection of the particles from the well. The field as a function of time roughly approximates the first 180° of a sine curve of period 3 μsec. Arrival time of the particles at the polarimeter varies by a maximum of 80 nsec (half a well period). During the run the basic machine rate averaged 4000 Hz, i.e., we injected, let the beam drift for the preset trapping time, and then ejected at this rate. Development of the pulsed coil was not trival. Details of the final coil construction and pulsing system have been published elsewhere.[13]

E. Vacuum

The trapping of positrons takes place in a 1-ft-diam aluminum vacuum section. A 650 liter/sec diffusion pump, and a 280 liter/sec Vacion pump were used to maintain a vacuum of less than 10^{-6} Torr in the trap. No particular effort was made to calibrate the ionization gauges used in the experiment. Absolute pressures are therefore uncertain to a factor of 2 or 3. Positrons were trapped for times up to 110 μsec. Scattering of the beam on neutral background gas is not an important effect in the experiment. More specifically, the trapping rate in the highly collimated system was not sensitive to vacuum pressure in the range of less than 10^{-6} Torr; also, the observed ω_D curve has about the same amplitude at the 110-μsec trapping time as at the 20-μsec trapping time, indicating negligible depolarization due to positron-atom collisions.

F. Detection and Control System

The coincidence, control, and recording setup is shown in Figs. 1–3. On ejection from the trap, positrons leave the vacuum section via a 15-mil Mylar window and enter the stopping scintillator (Fig. 1). This β^+ detector is a 9-mm-diam

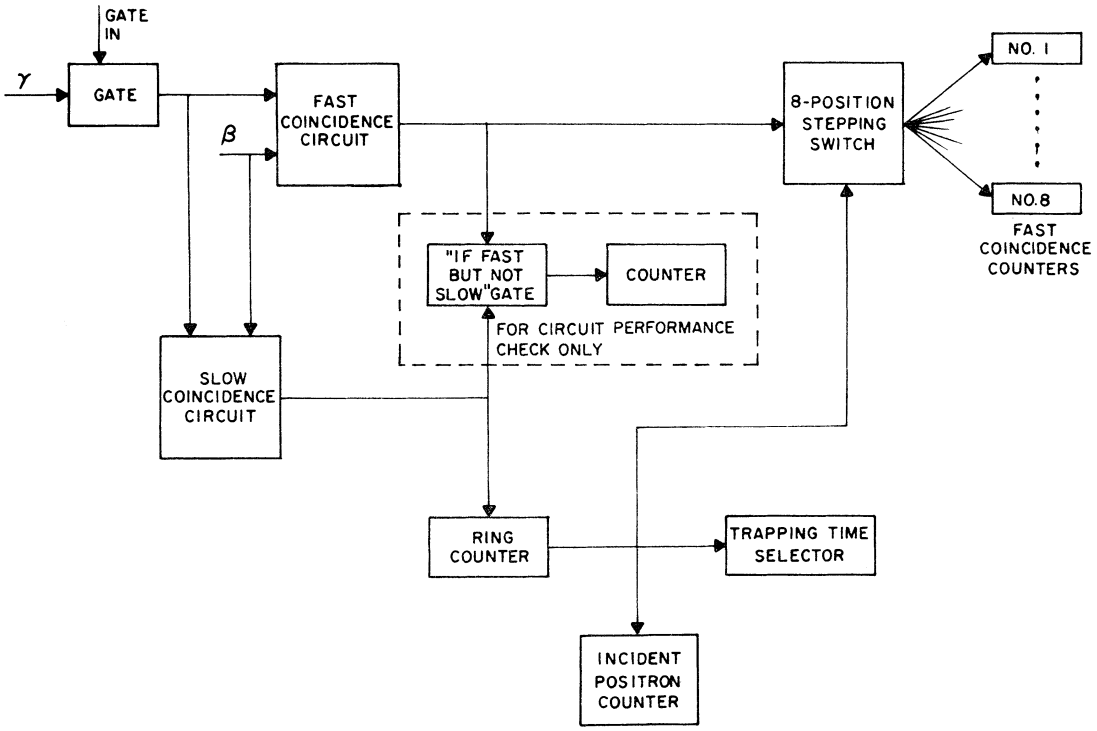

FIG. 2. Block diagram of the coincidence circuit and logic system. The symbols β and γ denote signals from the β and γ detectors.

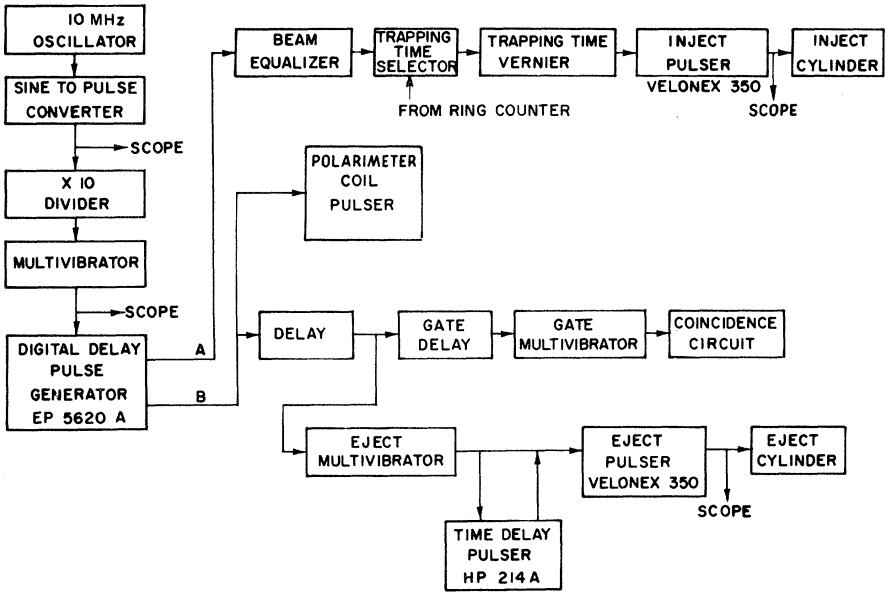

FIG. 3. Block diagram of the timing system. Function of the various components is explained in the text.

1-mm-thick disk of Naton 136 optically coupled to an RCA 8575 photomultiplier. One of the positronium decay γ's is detected by a $4\times8\times7$-in. Nation 136 scintillator coupled to an RCA 4522 photomultiplier. A complete description of the fast coincidence circuit (Fig. 2) is published elsewhere.[14]

The prompt curve $Q(t)$ of the fast coincidence circuit has a full width at half-maximum counting rate of about 4 nsec. If $f(\theta,t)$ is the theoretical distribution function, i.e., $f(\theta,t)=-(1/N_0)(dN/dt)dt$, with N as given in Eq. (3), then the expected polarimeter response is

$$F(\theta,t_1)=\int_{t_1}^{t_1+\Delta t}dt'\int_{-\infty}^{\infty}f(\theta,t')Q(t'-t)dt\,. \qquad (8)$$

Here t_1 is the time delay between positron thermalization and the opening of the coincidence gate of width Δt. Setting $t_1=3$ nsec and $\Delta t=12$ nsec, one arrives at

$$F(\theta)=(0.4\pm0.1)[1-(0.015\pm0.005)\cos\theta]\,. \qquad (9)$$

This is in agreement with the 2% asymmetry actually observed.

The slow coincidence circuit (Fig. 2), with 30-nsec-wide pulses in both channels, records the arrival of all positrons which give any sort of coincidence, either prompt or delayed. The output of the slow coincidence system is fed to a ring counter, which generates an output pulse for every third input pulse. The ring counter signal is then used to advance the trapping time and recording channel.

The pulse-timing system is shown in Fig. 3. This set of circuits controls the relative timing of the inject pulse, the eject pulse, the polarimeter coil pulse, and the gate pulse to the fast and slow coincidence systems. The trapping time is monitored by the simultaneous display on an oscilloscope of the inject pulse, eject pulse, and a 10-MHz timing pulse. The 10-MHz oscillator is controlled by an oven-heated crystal, and its frequency periodically checked against an independently calibrated Hewlett-Packard 445L frequency counter. The total uncertainty in trapping time, including drifts and measurement errors, is about ±0.014 μsec and is negligible compared to other sources of error.

The "time-delay pulser" shown at the bottom of the diagram serves to provide a second eject pulse for each machine cycle. As previously explained, the ejection process is only 50% efficient. A large carry-over of particles from one machine cycle to the next will cause a systematic distortion in the shape of the cosine curve. The second eject, combined with natural trapping losses, ensures that this carry-over is less than 3% of the total trapped beam.

Although beam drifts caused the trapping rate to vary somewhat with trapping time, a constant signal-to-noise ratio was maintained with a "beam equalizer." This device deletes inject triggers for a controlled percentage of machine cycles. The deletion can be adjusted for each channel separately. The effective trapping rate and signal-to-noise ratio are therefore the same for all trapping times, if the noise rate is independent of trapping time, and constant except for source decay and long-term detector drifts. Tests have shown this assumption to be valid. For example,

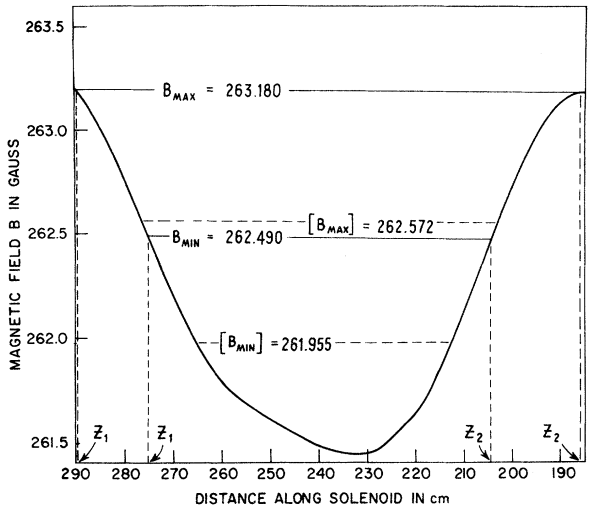

FIG. 4. Magnetic field in the trapping region at $r = 7.6$ cm.

no asymmetry is observed when the system is run with the incident positron beam blocked from the β^+ detector or with inject and eject pulses turned off.

γ rays from the sources accounted for 90% of the noise coincidences. Such coincidences resulted from Compton scattering of a γ ray in the β^+ detector with subsequent absorption of the same γ ray in the γ detector, or the inverse process. The random coincidence of a γ ray in the γ detector with a dark current pulse in the β^+ detector accounts for most of the remaining noise. All other sources of systematic and random coincidence noise are insignificant. The average signal-to-noise ratio during the runs was 8:1.

The system thus serves two purposes, which are (i) to normalize the delayed fast coincidence counts to the total number of detected positrons and (ii) to cycle the system against effects of slow drifts in the detection system and changes in source strength. If g were equal to 2, each channel would record the same number of fast coincidence counts.

IV. DATA AND ANALYSIS

A. Calculation of Time Average Field

In Fig. 4 we see an NMR map of the magnetic field in the trapping region. A trapped positron can move through, at most, a 1.6-G range of B values, or a total variation of about ± 3400 ppm. The maximum range of time-averaged fields which our distribution of particles in the well can experience is only about ± 1200 ppm. Here the time-averaged field $[B_z]$ is determined by the equation

$$[B_z] = 2\left(\int_{z_1}^{z_2} B(z)dt\right)\Big/ \tau_z(z_1, z_2)$$

$$= \int_{z_1}^{z_2} B_z(z)\frac{dz}{v_z(z)}\Big/\int_{z_1}^{z_2}\frac{dz}{v_z(z)} \ , \qquad (10)$$

where z_1 and z_2 are the axial limits of motion of a given positron, $\tau_z(z_1, z_2)$ is its period of oscillation, and $v_z(z)$ is its velocity at z. In order to derive an explicit expression for $[B_z]$, we consider the action integral $J = (1/2\pi)(e/\gamma m_0 c)\oint \vec{P}_\perp \cdot d\vec{l}$. Let R be the average radius of the helix of trapped particles. Assume that (i) the maximum fractional change of field within area πR^2 circumscribed by an orbital revolution of the positron is much less than 1; and (ii) the axial velocity component v_z is much less than the perpendicular velocity component $v_\perp$. Here $\vec{P}_\perp$ is the perpendicular component of the canonical momentum, i.e., $\vec{P}_\perp = \gamma m_0 \vec{v}_\perp + [(e)/c]\vec{A}$, with $\vec{A}$ the vector potential. Then J, an adiabatic invariant, is approximately given by $\pi c(\gamma m_0)^2 v_\perp^2/eB_z$. A more detailed treatment of the validity of this approximation is contained in Appendix IV of Ref. 15. This is the leading term in a series for J. The second term in the series is of order $[R/(z_2 - z_1)]^2$. Its omission causes a 25-ppm change in $[B_z]$. Since magnetic forces are perpendicular to particle velocities, the total velocity $|\vec{v}|$ is a rigorous constant of the motion. Thus $v_\perp^2/B_z(z)$ is an approximate adiabatic invariant, and we may write

$$v_z^2(z) = v^2 - v_\perp^2(z) = v^2 - \frac{B_z(z)}{B_z(z_0)}\, v_\perp^2(z_0) \ , \qquad (11)$$

where $B_z(z_0)$ and $v(z_0)$ are reference values of $B_z(z)$, and the total velocity is $v(z)$. Here we chose $z_0 = z_1$. Since $v_z(z_1) = 0$, we have $v_\perp(z_1) = v$ and

$$v_z(z) = \frac{v}{[B_z(z_1)]^{1/2}}\,[B_z(z_1) - B_z(z)]^{1/2} \ . \qquad (12)$$

Equation (10) then becomes

$$[B_z] = B_z(z_1) - \frac{\int_{z_1}^{z_2}[B_z(z_1) - B_z(z)]^{1/2}\,dz}{\int_{z_1}^{z_2} dz\,[B_z(z_1) - B_z(z)]^{-1/2}} \ . \qquad (13)$$

In the actual evaluation of $[B_z]$, we use $B = (B_z^2 + B_r^2)^{1/2}$ instead of B_z, since B is the quantity measured by the NMR mapper. The radial field B_r may be calculated from the approximate expression $B_r \sim R(\partial B/\partial z)$, where R is the orbit radius. For the parameters of our experiment we have $B_r/B_z \leq 10^{-3}$ or $(B - B_z)/B_z \approx 10^{-6}$.

B. Calculations of Ensemble Average $[B_z]$

The final major step in the determination of ω_0 is the calculation of the ensemble average $\langle[B]\rangle$. Specifically, we wish to evaluate

$$\langle[B]\rangle = \int_{B_{max}}^{B_{min}} \rho(B_i)\,[B_i]\,dB_i \ . \qquad (14)$$

Here $\rho(B_i)$ is the normalized density of particles at the level B_i, $[B_i]$ is the time-averaged field for a particle at the amplitude B_i, and $B_{\min}$ and $B_{\max}$ are the minimum and maximum amplitudes of the trapped particles.

In order to determine $\rho(B_i)$, we must further interpret Eq. (11). We first multiply both sides of the equation by the constant $\frac{1}{2}\gamma m_0$ to get

$$\tfrac{1}{2}\gamma m_0 v_z^2(z) = \tfrac{1}{2}\gamma m_0 v^2 - \frac{B_z(z)}{B_z(z_0)}\,\tfrac{1}{2}\gamma m_0 v_\perp^2(z_0)\ . \qquad (15)$$

Since γ is constant we identify $\frac{1}{2}\gamma m_0 v_z^2(z)$ with the axial kinetic energy $T_z(z)$ of the particle. The term axial kinetic energy is used in the sense that the work done by the axial component of magnetic force as the positron moves between z_0 and z is given by

$$\int_z^{z_0} (d/dt)\,(\gamma m_0 v_z)dz = \tfrac{1}{2}\gamma m_0[v_z^2(z_0) - v_z^2(z)].$$

Thus we have

$$T_z(z) - T_z(z_0) = [B_z(z_0) - B_z(z)]\,\frac{\frac{1}{2}\gamma m_0 v_\perp^2(z_0)}{B_z(z_0)}$$

$$= U(z_0) - U(z). \qquad (16)$$

This equation was used without derivation in Sec. III. It relates $B_z(z)$ to potential energy $U(z)$ through the constant $\frac{1}{2}\gamma m_0 v_\perp^2(z_0)/B(z_0)$, which is 866 eV/G for the parameters of our experiment. The distribution of particles in the well is obtained by measuring the number of particles (N) ejected from the well as a function of eject pulse height (E). The slope of an N-vs-E plot is simply converted to $\rho(B_i)$ using Eq. (16). This equation is not exactly valid because we do introduce an axial electric field in order to eject the positrons, thereby changing γ and hence $v_\perp^2$ slightly. In fact, however, we can convert from the eject voltage to B_i using Eq. (12) with an error of order $v_z^2/c^2 \approx 4\times10^{-4}$ as compared to unity.[16] A typical result for ρ is shown in Fig. 5. As discussed below, only a relatively crude knowledge of the form of ρ is required. The systematic change of ρ as a function of trapping time was negligible over the range of trapping times used in this experiment.

Systematic error in $\langle[B]\rangle$ from uncertainty in the quantity $T_\perp(z_0)/B_z(z_0)$ is due almost wholly to the 7% uncertainty in $\gamma v_\perp^2(z_0)$, i.e., $(\gamma - 1)m_0c^2 = 273 \pm 21$ keV. A recalculation of $\langle[B]\rangle$ assuming a 7% change in $T_\perp(z_0)/B_z(z_0)$ gives a result shifted by about 70 ppm. Note that this is an absolute maximum error in the sense that it assumes that particles used in the experiment had trajectories with radii 7.2 or 8.0 cm only. Such a situation is very unlikely. The ensemble average $\langle T_\perp(z_0)/B_z(z_0)\rangle$ could have been calculated to a much greater precision had the need existed and had the appropriate tests been conducted. Similarly, it was necessary

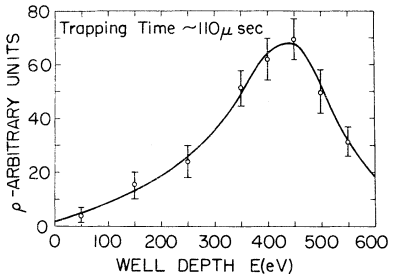

FIG. 5. Particle density as a function of depth in the magnetic well.

to measure the eject pulse height to only 10% since this leads to an uncertainty of only 100 ppm in $\langle[B]\rangle$.

A systematic error also results from the relatively "slow" rise time of the eject pulse. The rise time of the pulse and the half-period of the well are roughly equal. The effect is that an increase ΔE_i in eject (E_i) gives a change in counting rate not quite equal to the corresponding $\rho(B_i)\Delta B_i$. Instead, part of this change is due to an increase in ejection efficiency for particles at slightly higher levels. The effect has been considered in detail. Crude, but conservative, integration estimates place a 140-ppm upper bound on any possible shift in $\langle[B]\rangle$. Finally, a correction to account for the slight sensitivity of the detector to the pitch of the ejected beam is negligible (35 ppm).

The sensitivity of $\langle[B]\rangle$ to random counting errors in the experiment was simply estimated. Several curves were "poorly" fitted to the particle-distribution data points. Most of the points were made to fall a full standard deviation from the curve. An attempt was made to induce the largest possible shift in $\langle[B]\rangle$. The only restriction was that the curve be rather smooth. The maximum deviation was 70 ppm, and we take this as a conservative estimate of the uncertainty in $\langle[B]\rangle$ from random counting errors. The smallness of this error relative to the 1000-ppm uncertainty in ω_p and the unknown nonlinear functional form for ρ make a more mathematical treatment unworthwhile.

The total error in $\langle[B]\rangle$ from the ensemble-averaging process is 196 ppm. It is the square root of the sum of the squares of all of the above errors.

We quote the final value of $\langle[B]\rangle$ as $\langle[B]\rangle = 262.13$ $(1 \pm 212$ ppm) G. The error quoted is the square root of the sum of the squares of the standard deviations introduced by NMR field regulation (75 ppm), by NMR field mapping (30 ppm), and by the ensemble-averaging process (196 ppm). It is about $\frac{1}{5}$ of the statistical error in ω_p.

C. Determination of ω_p

Table I gives the output of the polarimeter (N_i) as a function of trapping time (T_i). The data were

TABLE I. Number of fast coincidence counts recorded (N_i) for each trapping time (T_i). Data for the three runs were taken in the order run I, run II, and then run III.

Run I		Run II	
Trapping time (T_i μsec)	N_i(counts)	Trapping time (T_i μsec)	N_i(counts)
15.278	7205	109.290	2917
15.572	7446	109.584	3005
15.866	7312	109.878	3007
16.160	7215	110.172	2893
16.453	7301	110.466	2923
16.747	7359	110.760	3039
17.041	7351	111.054	2934
17.335	7010	111.358	2906

Run III	
Trapping time T_i (μsec)	N_i(counts)
57.581	687
57.875	719
58.169	679
58.463	665
58.756	660
59.050	716
59.344	669
59.638	664

collected in three main runs numbered in the order in which they were performed.

Figure 6 is a normalized plot of the data for runs I and II. The two solid curves are least-squares fits to the eight points which determine each segment. Baseline (A), amplitude (B), and phase (ϕ) were the fitted parameters. Two successive fittings were made to each set of points. The first fit assumed the value of ω_D calculated from the results of the previous positron measurement. The 0.5% uncertainty in this value introduces an extra 1.5° uncertainty in the best fit value of ϕ for each curve, as ascertained by fitting curves for several assumed values of ω_D. Such an uncertainty is almost negligible when compared to statistical counting errors (see below).

An improved value of $\tau_D = 2\pi/\omega_D$ is then calculated. This is done by dividing the time (ΔT) between the zero phase points T_1 and T_2 shown in Fig. 6 by the number of cycles (80) between them. This yields a value of ω_D accurate to about 0.1%, which is then used in a second fit of the curves. The error in phase introduced by the above uncertainty in ω_D is now a truly negligible 0.3°. Using these slightly refined values of T_1 and T_2, we then have $\tau_D = (T_1 - T_2)/80 = (109.363 - 15.327)/80$ μsec = 1.1754 μsec as our final value.

Error in ΔT is primarily due to statistical uncertainty in ϕ. The standard deviation $\sigma(\phi)$ in the phase of the curves was computed using the method of maximum likelihood. The resulting expression $\sigma(\phi) \approx B\sqrt{2}/A\sqrt{N_T k}$, where N_T is the total number of counts in the record. The error theory involved here is discussed in Ref. 5. The results from runs I and II are $\sigma_1(\phi) = 16°$ (0.053 μsec) and $\sigma_2(\phi) = 23.8°$ (0.078 μsec).

As a further check, we plotted the value of the likelihood function vs phase ϕ, using best-fit values for baseline and frequency. The resulting curves are very nearly Gaussian, with half-widths at half-maximum of 15° for run I and 18° for run II. Finally, we broke the data for each run into n separate groups and fitted a cosine curve to each group. The standard deviation of the mean, $\overline{\phi}$, of the n phases is given by the equation

$$\sigma^2(\overline{\phi}) = [n(n-1)]^{-1} \sum_{i=1}^{n} (\phi_i - \phi)^2 ,$$

where n is the number of data points. For run I, $n = 13$ and $\sigma(\overline{\phi}) = 16°$, while for run II, $n = 10$ and $\sigma(\overline{\phi}) = 18°$.

We use the results of the likelihood calculations as our most conservative estimate of error. Statistical error in τ_D is then $\tau_D = (0.052^2 + 0.078^2)^{1/2}/80$ μsec = 0.0017 μsec, or 995 ppm of τ_D itself. Systematic error in ΔT associated with time measurement and control is ±0.014 μsec or about 168 ppm as noted in Sec. III. This results mainly from the limitations of our measuring trapping times with an oscilloscope. Our final value of τ_D is then $\tau_D = 1.1754$ (1 ± 1010 ppm) μsec.

The above assumes a knowledge of the true number of cycles N in ΔT. The location of the zero phase point T_2 fell within 0.08 cycles of the point predicted by theory. Nevertheless, in performing the experiment one must predict the location of T_2 from T_1 using the experimental value from the Rich and Crane experiment, for which the quoted uncertainty in $a_E(e^+)$ is 0.5%. This is the dominant source of error in the prediction of the value of T_2. Specifically, $T_2 = T_1 + 80\tau_D$, where τ_D is the value calculated from $a_E(e^+)$. The 0.052-μsec uncertainty in T_1 corresponds to only 16°, while the uncertainty in 80 τ_D is ~0.4 cycles or 144°. Thus

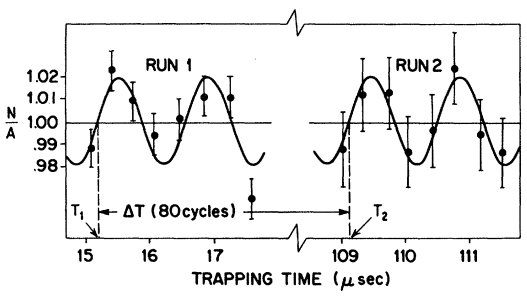

FIG. 6. Best-fit curves $N/A = 1 + (B/A)\cos(\omega_D T + \varphi)$ to the normalized data for runs I and II.

the predicted zero phase point T_2 is uncertain by 145° (0.4 cycles). The measured T_2 fell about midway between the zero phase points predicted for $N=80$ and $N=81$. More exactly, the measured T_2 fell about 0.58 cycles or 1.45 standard deviations from the predicted zero phase point for $N=80$, and about 0.42 cycles or 1.05 standard deviations from that for $N=81$.

At this point, therefore, $N=81$ was about twice as likely as $N=80$, i.e., the probability of being off by 1.05 standard deviations is about twice that of being off by 1.45 standard deviations. All other values of N are very unlikely as they represent departures of 3.55 standard deviations or more.

In order to select the correct value of N, we took data for another eight-point curve (run III) about midway in trapping time between T_1 and T_2. The phase of the curve was that which we expected if $N=80$. Since only about 600 counts per point were collected for run III, the average normalized amplitude of runs I and II was used to calculate $\sigma(\phi) = B\sqrt{2}/A\sqrt{N_T} = 58°$ for run III. Also, the validity of using this formula at only a 600 count per point level was tested directly. The more voluminous data of the Rich and Crane experiment were broken up into 100 runs with roughly 600 counts per point. A histogram plot of the number of fits vs the corresponding value of ϕ was made. The plot corresponded well to a Gaussian with the full width at half-maximum predicted by the maximum likelihood calculation.

The probability that the phase of run III is off by 180° is about 0.002, since this corresponds to a 180°/58° or 3.1-standard-deviation discrepancy. Thus the relative probability for $N=81$ is about 0.004 of that for $N=80$. It should be noted that if a 1-cycle miscount occurs, i.e., if the true number of cycles is 81, our experiment disagrees with theory by about 10 standard deviations. More data taken during run III would, of course, increase our confidence in the $N=80$ result; however, the experimental constraint of a low counting rate prevented further data accumulation.

V. CALCULATION OF THE g FACTOR

A. Anomaly Without Correction

The value of a without correction terms is

$$a = \langle[\omega_D]\rangle/\langle[\omega_0]\rangle = 2\pi(m_0c/e)_{e^+} + [\langle\tau_D\rangle\langle[B_z]\rangle]^{-1} .$$

Here we assume $(m_0/e)_{e^-} = (m_0/e)_{e^+}$. This assumption is valid for our measurement since it has been shown experimentally[8] that

$$(m_0/e)[(e/m_0)_{e^-} - (e/m_0)_{e^+}] = (26 \pm 71) \times 10^{-6} .$$

The error in $\langle[\omega_D]\rangle/\langle[\omega_0]\rangle$ is then essentially the square root of the sum of the squares of the errors in $\langle[\tau_D]\rangle$ and $\langle[B_z]\rangle$, or 1030 ppm.

B. Finite-Pitch Correction

For evaluation of the finite-pitch correction term, $\frac{1}{2}a[v_z^2]/c^2$, we use

$$[v_z^2] = \frac{v^2}{B(z_1)} \int_{z_1}^{z_2} [B(z_1) - B(z)]^{1/2}\, dz \Big/ \int_{z_1}^{z_2} \frac{dz}{[B(z_1) - B(z)]^{1/2}} . \quad (17)$$

This relation follows simply by substituting the expression for v_z given by Eq. (7) into

$$[v_z^2] = \frac{1}{\tau_z}\int_{t_1}^{t_2} v_z^2\, dt = \int_{z_1}^{z_2} v_z\, dz \Big/ \int_{z_1}^{z_2} \frac{dz}{v_z} .$$

The ensemble average of $[v_z^2]$ is then calculated in a manner identical to that discussed above for $\langle[B_z]\rangle$. The result is $\frac{1}{2}a\langle[v_z^2/c^2]\rangle = (8.3 \pm 0.5) \times 10^{-7}$, where we have used $a = 0.00116$. Note that this correction term shifts the value of a by less than 1000 ppm, which is the order of the error in ω_D. The 50-ppm error in the term is due almost entirely to the 5.5% uncertainty in total velocity v.

C. Radial-Electric-Field Correction

In stating the final value of a, we shall assume that the $\langle[E_r]\rangle$ correction as given by Eq. (6) is negligible. A 1-standard-deviation shift in our result would require that the value of $\langle[E_r]\rangle$ be 0.15 V/cm. We will show, in the remainder of this section, that such a value is improbably high.

As far as electric fields are concerned, the principal difference between e^+ and e^- work at our laboratory is the use of a radioactive source rather than an electron gun. The geometry, materials in the vacuum sections and cylinders, pumping technique, pressure, etc., are almost identical. In their e^- experiment, Wilkinson and Crane were able to measure a at several different values of B and from the data infer that $\langle[E_r]\rangle$ was about -0.003 V/cm. Low counting rates ruled out such a procedure in our work, but we note, from Eq. (6), that a field of -0.003 V/cm would result in only a 20-ppm shift in our value of a.

We can, in addition, make order-of-magnitude estimates of the $\langle[E_r]\rangle$ generated by the following source-related mechanisms[17]:

a. Beam space charge. The probability of having more than one e^+ trapped in the well at the same time is less than 10^{-4}. The dc beam from the source is about $10^5 e^+$/sec, while the maximum time of passage across the well is about 10^{-7} sec. Thus the chance of finding a positron in the trapping region at any given time is about 10^{-2}.

b. Ionization. (i) The specific ionization of 272-keV positrons in air is about 20 ion pairs/cm at STP. After scaling to a pressure of 10^{-6} Torr

we find that the total ionization rate from both the trapped and dc beams is less than 30 ion pairs/sec. About 10^9 ion pairs must be present inside the beam radius to produce an $\langle[E_r]\rangle$ of 0.15 V/cm. This very conservative estimate assumes complete separation of charge, i.e., the electrons escape immediately from the trapping region while the positive ions are trapped indefinitely with negligible recombination probability. Even under such improbable conditions, it would take several years to build up the required charge density when source decay is also considered. (ii) The unimportance of gas ionization by the beam may also be seen by a comparison with the Wilkinson and Crane experiment. A calculation of the ion-pair production rate, similar to the one just outlined, was performed for the electron experiment. The result is that at least 10^4 more ions/sec must have been produced in the electron experiment than in the positron experiment. Thus since $\langle[E_r]\rangle$ from this source was small in the former experiment, it was quite probably negligible in the latter. (iii) The ionization of residual gases in the trap by γ radiation is also insignificant. The 0.8-MeV γ rays which pass directly from the sources to the trapping region can account for an ion-pair production rate which is only of the order of 10^{-2}/sec. The ionization by the 0.511-MeV γ rays from positron-electron annihilation is about four times smaller. Multiple scattering of these γ rays from the cylinder walls and other pieces of apparatus does not change this result insignificantly. Finally, the x-ray production occurring in the collimator and cylinder wall is similarly insignificant.

c. Photoelectrons and Compton electrons. The total of such charge within the trapped-beam radius at any given time must be quite small. More specifically, even if all the energy emitted per second by the sources were to go into the production of electrons capable of passing inside the beam radius, one can show that only a few hundred electrons would reside there at any given instant.

d. Charging of metallic surfaces by the sources. This effect results from the presence of dielectric impurities on the surface of the trapping cylinders, collimator, etc. Since the maximum possible thickness of a dielectric impurity, for example, diffusion pump oil, on these surfaces is about 10^{-5} cm, any charging capable of supporting a 0.15-V/cm field seems quite unlikely. Nonetheless, an auxiliary experiment was performed to test for such charging.

The test is based on the motion of the untrapped beam as it traverses the well. As an example, a difference in potential between the collimator and ejection cylinder not only implies the presence of a radial electric field in the trap, but also that of an axial component of field, E_z. Thus the equivalent potential depth of the trap is changed. This change is detected by the use of an auxiliary coil wound about the solenoid at the location of the right trapping peak ($z = 158$ cm in Fig. 1). The counting rate in the β detector is monitored as a function of the current in the auxiliary coil. As the magnetic hill at $z = 158$ cm is raised no change in counting rate should be observed until it reaches the level of the slightly higher left-hand peak. At this point, the right peak should begin to reflect positrons and a decrease in counting rate should be observed. Any departure from this may be interpreted as due to the presence of an electric field.

A combination of such tests for various assumed distributions of charge was performed. No potential shifts were detected. The resolution of the tests was about 15 eV. This implied a maximum E_r in the well of about (0.2 ± 0.1) V/cm or an $\langle[E_r]\rangle$ of about (0.12 ± 0.06) V/cm. This corresponds to ruling out shifts greater than about one standard deviation.

e. E_r not related to the source. A contact potential of 0.3 V is theoretically possible between the brass trapping cylinders and an aluminum facing on the collimator. Even assuming that the potential difference is maintained at its full theoretical value, it corresponds to an $\langle[E_r]\rangle$ of only about 2 mV/cm. The problem of the patch effect as a source of electric field has been considered in experiments on the free fall of the electron.[18] Such a contribution to $\langle[E_r]\rangle$ in our system is truly negligible.

D. Miscellaneous Corrections

Further effects which we have considered and found to be unimportant are variation of the earth's field, changes in solenoid geometry with changes in temperature, magnetic contamination of the apparatus inside the solenoid, and possible phase shifts in $\vec{P}$ not due to ω_D. In a neighboring laboratory, the solenoid for the new electron g-factor experiment was turned on and off several times during our runs. Its fringe field changed the field in the trap of the positron experiment by less than 30 ppm. Finally, maps over the whole volume of the trap showed that effects on $\langle[B]\rangle$ from any possible radial drifting of the beam in the trap are insignificant.

E. Conclusions

Our result for the positron g-factor anomaly may be written as

$$a(e^+)E = \frac{\langle[\omega_D]\rangle}{\langle[\omega_0]\rangle} + \tfrac{1}{2}a\frac{\langle[v_z^2]\rangle}{c^2} = (11\,603 \pm 12) \times 10^{-7}$$

or

$$a(e^+)_E = \alpha/2\pi - (0.24 \pm 0.22)\alpha^2/\pi^2 .$$

This result is five times more accurate than the best previous positron determination. Thus the positron g factor is equal to both the theoretical and experimental value of the electron g factor at the 1-ppm level. Furthermore, since the μ^+ and μ^- g factors are equal to within 0.7 ppm, any violation of *TCP* which manifests itself in a lepton-antilepton g factor asymmetry is ruled out at the 1-ppm level.

This measurement has pushed the present experimental technique to the point of diminishing returns. Low-beam intensity is the foremost problem. Significant improvement over the present experiment awaits the invention of techniques which make more efficient use of the positron source or which increase the efficiency of the polarimeter.

ACKNOWLEDGMENTS

We would like to thank Professor H. R. Crane, Professor D. M. Dennison, Professor G. W. Ford, Professor H. C. Griffin, Professor R. R. Lewis, and Dr. J. C. Wesley for informative discussions and advice. R. O. Roth and G. Yanik performed much valuable day-to-day work on the apparatus. The Co^{58} sources were fabricated to our rather demanding specifications by the Nuclear Science and Engineering Corporation.

APPENDIX: POSITRONIUM

1. Purpose of Appendix

The objectives of this Appendix are: (i) to give a simplified and approximate calculation of the expressions for the decay rates (Λ) of the field perturbed states of Ps; (ii) to list the values of the decay constants required for the calculation of N as given by Eq. (3) in Sec. II; (iii) to provide an intuitive explanation of why the lifetime distribution of Ps in a magnetic field should depend in any manner upon the polarization of the incident beam.

2. Decay Constants of Positronium

In this treatment we shall not include an explicit discussion of the radiation correction term. We shall assume that the Hamiltonian H for positronium in a magnetic field is given by

$$H = H_0 + H_M , \tag{A1}$$

where H_0 includes the hyperfine interaction. Further, we may write

$$H_0 \Psi_{F,m} = E_F \Psi_{F,m} , \tag{A2}$$

where $\Psi_{F,m}$ are the eigenstates of the stationary ground state of the system when $H_M = 0$. The quantum number $F = 0, 1$ denotes the spin state of the atom, and m denotes the z component. These states, when expanded in terms of the spin states of the individual particles, are (Φ_0 is the space component)

$$\begin{aligned}
&\Psi_{1,1} = \Phi_0 S_e(\uparrow) S_p(\uparrow) , \\
&\Psi_{1,0} = (\Phi_0/\sqrt{2})[S_e(\uparrow) S_p(\downarrow) + S_e(\downarrow) S_p(\uparrow)] , \\
&\Psi_{1,-1} = \Phi_0 S_e(\downarrow) S_p(\downarrow) , \\
&\Psi_{0,0} = (\Phi_0/\sqrt{2})[S_e(\uparrow) S_p(\downarrow) - S_e(\downarrow) S_p(\uparrow)] .
\end{aligned} \tag{A3}$$

Here $S_e(\uparrow)$ refers to the spin-up state of the electron, $S_p(\downarrow)$ the spin-"down" state of the positron, etc.

The interaction of the system with an external magnetic field B is represented by H_M. In terms of the Pauli spin matrices σ_z, H_M may be written as

$$H_M = \tfrac{1}{2}\mu_B g B (\sigma_{ez} - \sigma_{pz}) . \tag{A4}$$

Direct evaluation of the elements $\langle \Psi_{F,m} | H | \Psi_{F',m'} \rangle$ then gives the Hamiltonian matrix

$$(H) = \begin{pmatrix} E_1 & 0 & 0 & 0 \\ 0 & E_1 & 0 & \mu_B g B \\ 0 & 0 & E_1 & 0 \\ 0 & \mu_B g B & 0 & E_0 \end{pmatrix} . \tag{A5}$$

Solution of the secular equation for (H) gives the diagonalized matrix $(H)_D$

$$(H)_D = \begin{pmatrix} E_1 & 0 & 0 & 0 \\ 0 & \overline{E} + \tfrac{1}{2}\Delta E (1+x^2)^{1/2} & 0 & 0 \\ 0 & 0 & E_1 & 0 \\ 0 & 0 & 0 & \overline{E} - \tfrac{1}{2}\Delta E (1+x^2)^{1/2} \end{pmatrix} . \tag{A6}$$

Here $\overline{E} = \tfrac{1}{2}(E_0 + E_1)$, $\Delta E = E_1 - E_0$, and $x = 2\mu_B g B/\Delta E$.

If (S) is the unitary transformation matrix which diagonalizes (H), then the field perturbed wave functions $\Psi'_{F,m}$ are given by

$$\begin{pmatrix} \Psi'_{1,1} \\ \Psi'_{1,0} \\ \Psi'_{1,-1} \\ \Psi'_{0,0} \end{pmatrix} = (S) \begin{pmatrix} \Psi_{1,1} \\ \Psi_{1,0} \\ \Psi_{1,-1} \\ \Psi_{0,0} \end{pmatrix} . \tag{A7}$$

The result is

$$\begin{aligned}
&\Psi'_{1,1} = \Psi_{1,1} , \\
&\Psi'_{1,0} = a\Psi_{1,0} + b\Psi_{0,0} , \\
&\Psi'_{1,-1} = \Psi_{1,-1} , \\
&\Psi'_{0,0} = a\Psi_{0,0} - b\Psi_{1,0} ,
\end{aligned} \tag{A8}$$

where

$$a = \frac{1}{\sqrt{2}} \left[1 + \left(\frac{1}{(1+x^2)^{1/2}}\right)\right]^{1/2} ,$$

$$b = \frac{1}{\sqrt{2}} \left[1 - \left(\frac{1}{(1+x^2)^{1/2}}\right)\right]^{1/2} .$$

TABLE II. Perturbed decay rates $\Lambda'_{F,m}$ in terms of $\Lambda_{F,m}$ and $x \equiv 4\mu_B B_p/E_{1,0} - E_{0,0}$. Values for $B_p = 0$ and $B_p = 10$ kG are given for Ps formation in Naton 136.

Decay rates for positronium		
Expression for $\Lambda'_{F,m}$	Value of $\Lambda'_{F,m}$	Value for $\Lambda'_{F,m}$
	$B_p = 0$	$B_p = 10$ kG
$\Lambda'_{1,1} = \Lambda_{1,1}$	5×10^8 sec^{-1}	5×10^8 sec^{-1}
$\Lambda'_{1,0} = \frac{1}{2}(\Lambda_{1,0}+\Lambda_{0,0}) + (1+x^2)^{-1/2}\frac{1}{2}(\Lambda_{1,0}-\Lambda_{0,0})$	5×10^8 sec^{-1}	7×10^8 sec^{-1}
$\Lambda'_{1,-1} = \Lambda_{1,-1}$	5×10^8 sec^{-1}	5×10^8 sec^{-1}
$\Lambda'_{0,0} = \frac{1}{2}(\Lambda_{1,0}+\Lambda_{0,0}) - (1+x^2)^{-1/2}\frac{1}{2}(\Lambda_{1,0}-\Lambda_{0,0})$	8×10^9 sec^{-1}	7.8×10^9 sec^{-1}

We then have the annihilation rate $\Lambda'_{F,m}$ of the field perturbed states in terms of the $\Lambda_{F,m}$:

$$\Lambda'_{1,1} = \Lambda_{1,1}\,, \qquad \Lambda'_{1,0} = a^2\Lambda_{1,0} + b^2\Lambda_{0,0}\,,$$
$$\Lambda'_{1,-1} = \Lambda_{1,-1}\,, \qquad \Lambda'_{0,0} = a^2\Lambda_{0,0} + b^2\Lambda_{1,0}\,. \tag{A9}$$

In Table II we see $\Lambda'_{1,0}$ and $\Lambda'_{0,0}$ expressed in terms of the parameter x. Evaluations for Ps in Naton 136 and $B_p = 10$ kG are also given.

3. Positronium Polarimeter

Here our purpose is to present an intuitive discussion of the polarimeter. For useful quantitative expressions, see Ref. (12).

Assume we allow B to increase until the energy separation of the $m = 0$ singlet and triplet states is much greater than the hyperfine interaction. From Eqs. (3) and (8), the possible wave functions for the system, written in terms of individual particle spin states, approach

$$\Psi'_{1,1} \to \Phi_0 S_e(\uparrow) S_p(\uparrow)\,,$$
$$\Psi'_{1,0} \to \Psi_0 S_e(\uparrow) S_p(\downarrow)\,,$$
$$\Psi'_{1,-1} \to \Phi_0 S_e(\downarrow) S_p(\downarrow)\,, \tag{A10}$$
$$\Psi'_{0,0} \to \Psi_0 S_e(\downarrow) S_p(\uparrow)\,.$$

If we further assume that the positron beam is totally polarized "down", than the system is made up almost wholly of $m = 0$ triplet and $m = -1$ triplet. If the beam is totally polarized "up," then the system goes for all practical purposes entirely into $m = +1$ triplet and the singlet state. As the $m = 0$ triplet and singlet states decay at different rates for all but truly infinite fields, the lifetime distribution is seen to depend upon the initial polarization of the positron beam.

*Work supported by the U. S. Atomic Energy Commission.

†Present address: Gulf Energy and Environmental Systems, Inc., San Diego, Calif.

[1]See H. R. Crane, Sci. Am. 218, No. 1 (1966) for a history of these measurements.

[2]J. R. Gilleland and A. Rich, Phys. Rev. Letters 23, 1130 (1969).

[3]J. Bailey, W. Bartl, G. Von Bochmann, R. C. A. Brown, F. J. M. Farley, H. Jöstlein, E. Picasso, and R. W. Williams, Phys. Letters 218B, 287 (1968).

[4]A. Rich and H. R. Crane, Phys. Rev. Letters 17, 271 (1966).

[5]J. C. Wesley and A. Rich, Phys. Rev. A 4, 1341 (1971).

[6]G. R. Henry and J. E. Silver, Phys. Rev. 180, 1262 (1969); A. Rich, Phys. Rev. Letters 20, 968 (1968); 21, 1221(E) (1968).

[7]B. N. Taylor, W. H. Parker, and D. N. Langenberg, Rev. Mod. Phys. 41, 375 (1969).

[8]L. A. Page, P. Stehle, and D. B. Gunst, Phys. Rev. Letters 89, 1273 (1953).

[9]The polarimeter was first suggested by V. L. Telegdi; see L. Grodzins, Progr. Nucl. Phys. 7, 219 (1959). It was first demonstrated by L. Dick, L. Feuvrais, and V. L. Telegdi, Aix-en-Provence International Conference on Elementary Particles, 1961, Vol. VI, p. 295 (unpublished). One of us (A. R.) wishes to thank Professor R. R. Lewis for bringing it to his attention.

[10]See Ref. 5 or J. C. Wesley and A. Rich, Phys. Rev. Letters 24, 1320 (1970).

[11]D. T. Wilkinson and H. R. Crane, Phys. Rev. 130, 852 (1963).

[12]For details on the effects of source thickness and backing on beam polarization, see A. Rich, thesis (University of Michigan, 1965) (unpublished), available from University Microfilms, Publication No. 66-6685.

[13]R. O. Roth and J. R. Gilleland, Rev. Sci. Instr. 39, 1696 (1968).

[14]A. Rich, thesis (University of Michigan, 1965) (unpublished), available through University Microfilms, Publication No. 66-6685, p. 46.

[15]J. R. Gilleland, thesis (University of Michigan, 1969) (unpublished), available through University Microfilms.

[16]The order of magnitude of the error made in using Eq. (12) in the presence of an electric field may be estimated by considering the relativistic motion of a particle moving in parallel $\vec{E}$ and $\vec{B}$ fields, if during the course of the motion the condition $\vec{v}\cdot\vec{E}/cB \ll 1$ obtains. For the exact solution see J. D. Jackson, *Classical Electrodynamics* (Wiley, New York, 1962), p. 427.

[17]For more detailed discussion of electric field estimates, see J. R. Gilleland, Ref. 15, pp. 52–68.

[18]C. F. Witteborn, thesis (Stanford University, 1965) (unpublished), available from University Microfilms, Ann Arbor, Publication No. 65-12, p. 888.